

1 Application of regional meteorology and air quality models 2 based on MIPS and LoongArch CPU Platforms

3
4 Zehua Bai^{1,2}, Qizhong Wu^{1,2}, Kai Cao^{1,2}, Yiming Sun³, Huaqiong Cheng^{1,2}

5
6 ¹College of Global Change and Earth System Science, Faculty of Geographical Science,
7 Beijing Normal University, Beijing 100875, China.

8 ²Joint Center for Earth System Modeling and High Performance Computing, Beijing
9 Normal University, Beijing 100875, China.

10 ³Beijing Institute of Talent Development Strategy, Beijing 100032, China.

11
12 **Correspondence:** Qizhong Wu (wqizhong@bnu.edu.cn)

13
14 **Abstract.** The Microprocessor without interlocked piped stages (MIPS) and
15 LoongArch are Reduced Instruction Set Computing (RISC) processor architectures,
16 which have advantages in terms of energy consumption and efficiency. There are few
17 studies on the application of MIPS and LoongArch CPUs in the geoscientific numerical
18 models. In this study, Loongson 3A4000 CPU platform with MIPS64 architecture and
19 Loongson 3A6000 CPU platform with LoongArch architecture were used to establish
20 the runtime environment for the air quality modelling system Weather Research and
21 Forecasting–Comprehensive Air Quality Model with extensions (WRF-CAMx), in
22 Beijing-Tianjin-Hebei region. The results show that the relative errors for the major
23 species (NO₂, SO₂, O₃, CO, PNO₃ and PSO₄) between the MIPS and X86 benchmark
24 platform are within ±0.1%. The maximum Mean Absolute Error (MAE) of major
25 species ranged to 10⁻² ppbV or μg m⁻³, the maximum Root Mean Square Error (RMSE)
26 ranged to 10⁻¹ ppbV or μg m⁻³, and the Mean Absolute Percentage Error (MAPE)
27 remained within 0.5%. The CAMx takes about 195 minutes on Loongson 3A4000 CPU,
28 71 minutes on Loongson 3A6000 CPU and 66 minutes on Intel Xeon E5-2697 v4 CPU,
29 when simulating a 24h-case with four parallel processes using MPICH. As a result, the

Deleted: MIPS processor architecture is a type

Deleted: of

Deleted: has

Deleted: was

Deleted: WRF-CAMx

Deleted: The CAMx takes about 15.2 minutes on Loongson 3A4000 CPU and 4.8 minutes on Intel Xeon E5-2697 v4 CPU, when simulating a 2h-case with four parallel processes using MPICH.

39 single-core computing capability of Loongson 3A4000 CPU for the WRF-CAMx
40 modeling system is about one-third of Intel Xeon E5-2697 v4 CPU and Loongson
41 3A6000 CPU is slightly lower than Intel Xeon E5-2697 v4 CPU, but the thermal design
42 power (TDP) of Loongson 3A4000 is 40W, while the Loongson 3A6000 is 38W, only
43 about one-fourth of Intel Xeon E5-2697 v4, whose TDP is 145W. The results also verify
44 the feasibility of cross-platform porting and the scientific usability of the ported model.
45 This study provides a technical foundation for the porting and optimization of
46 numerical models based on MIPS, LoongArch or other RISC platforms.

Deleted: 30

Deleted: one-fifth

Deleted: which

Deleted: Thus, Loongson 3A4000 has higher energy efficiency in the application of the WRF-CAMx modeling system. ...

47

48 **1 Introduction**

49 In the recent years, with the increasing demand for high-performance computing
50 resources and rapid development in the computer industry, especially supercomputer,
51 central processing unit (CPU) has undergone significant advancements in logical
52 structure, operational efficiency, and functional capabilities, making it the core
53 component of current computer technology development. There are two main types:
54 one is complex instruction set computer (CISC) CPU (George, 1990; Shi, 2008), mainly
55 using X86 architecture, representative vendors including Intel, AMD, etc., and widely
56 used in high-performance computing platforms. The other is reduced instruction set
57 computer (RISC) CPU (Mallach, 1991; Liu et al., 2022), mainly using ARM, MIPS,
58 RISC-V and other architectures, representative vendors including Loongson, etc., and
59 mainly used in high-performance computing platforms, which have high efficiency,
60 excellent stability and scalability. The Microprocessor without interlocked piped stages
61 (MIPS) architecture is one of the significant representatives of RISC architecture. MIPS
62 was originally developed in the early 1980s by Professor Hennessy at Stanford
63 University and his group (Hennessy et al., 1982). The simplicity of the MIPS instruction
64 set contributes to its ability to process instructions quickly, thus achieving higher
65 performance even in low-power conditions. In 1999, MIPS Technology Inc. released
66 the MIPS32 and MIPS64 architecture standard (MIPS Technology Inc., 2014).
67 Compared to the CISC CPUs, RISC CPUs demonstrate excellent performance and

74 power efficiency, which have gained popularity among chip manufacturers.

75 The Loongson processor family developed by Loongson Technology is mainly
76 designed using MIPS architecture and Linux operating system (Hu et al, 2011), which
77 has rich application tools in Linux open-source projects. The main reason that currently
78 restricts the development of CPUs that implement non-X86 instruction set architecture
79 such as MIPS64 is the immature software ecosystem (Hu et al., 2016). Based on the
80 strategy of open-source software, Loongson platform has gained abundant software
81 tools, making it possible to further develop scientific computing and numerical models.

82 Air quality model (AQM) systems use mathematical equations and algorithms to
83 simulate and predict the pollutant concentration in the atmosphere. The current AQMs
84 have become more complex, incorporating numerous factors such as emissions from
85 industrial sources, vehicle traffic, and natural sources, as well as meteorological
86 conditions, including modeling meteorology, emissions, chemical reactions, and
87 removal processes (Zhang et al., 2012). Regional-scale AQMs have been widely used
88 to predict air quality in cities, formulate emission reduction strategies, and evaluate the
89 effectiveness of control policies (Wang et al., 2023), including the Community
90 Multiscale Air Quality (CMAQ) modelling system (Appel et al., 2017; Appel et al.,
91 2021), the Comprehensive Air Quality Model with extensions (CAMx; RAMBOLL
92 ENVIRON Inc., 2014), and the Nested Air Quality Prediction Modeling System (Wang
93 et al., 2006; Chen et al., 2015). Due to the requirement of meteorological input,
94 commonly used offline meteorological models such as WRF (Michalakes et al., 2001)
95 are coupled offline with the regional AQMs to provide meteorological and chemical
96 forecast as the WRF-AQM modeling system, such the WRF-CMAQ modeling system
97 (Wu et al., 2014).

98 Both the meteorological and air quality numerical simulation rely heavily on high-
99 performance computing systems. The WRF-AQM systems can run stably on high-
100 performance computing platforms based on X86 or X86-compatible instruction set
101 architecture (ISA) CPUs, which account for the highest percentage among the main
102 processors of current high performance computing platforms. There are relatively
103 limited researches on the application of WRF-AQM system on MIPS [and LoongArch](#)

104 CPU platforms at present, this study focuses on the application of WRF-CAMx model
105 on Loongson CPU platform based on the MIPS [and LoongArch](#) architectures. A
106 simulation case covering the Beijing-Tianjin-Hebei region was set up to evaluate the
107 differences and performance between MIPS and X86 platforms. This study validated
108 the stability of scientific computing on MIPS [and LoongArch](#) CPU platform, and it
109 offered technical references and evaluation methods for the porting and application of
110 numerical models on non-X86 platforms.

111 Section 2 provides the model descriptions of the Weather Research and
112 Forecasting-Comprehensive Air Quality Model with extensions (WRF-CAMx)
113 modeling system, and the descriptions of MIPS, [LoongArch](#) and benchmark platforms.
114 The configuration of the air quality numerical simulation system and simulation case
115 are also presented in Section 2. Section 3 describes porting and optimization of the
116 WRF-CAMx modelling system on MIPS [and LoongArch](#) CPU platforms. Section 4
117 analyzes the differences of model results between MIPS CPU platform and the
118 benchmark platform. Section 5 discusses MIPS [and LoongArch](#) CPUs performance in
119 scientific computing. The conclusions are presented in Section 6.

120

121 2 Model and Porting Platform Description

122 The air quality modeling system was constructed using the WRF v4.0 model
123 developed by National Center for Atmospheric Research (NCAR) (Skamarock et al.,
124 2019), and the CAMx v6.10 developed by Ramboll Environment (RAMBOLL
125 ENVIRON Inc., 2014), as shown in Figure 1. And the Loongson 3A4000 CPU platform
126 was chosen for the porting work in the study. This study introduced the porting of WRF-
127 CAMx modeling system to MIPS [and LoongArch](#) CPU platforms.

Deleted:

Deleted: The remainder is organized as follows.

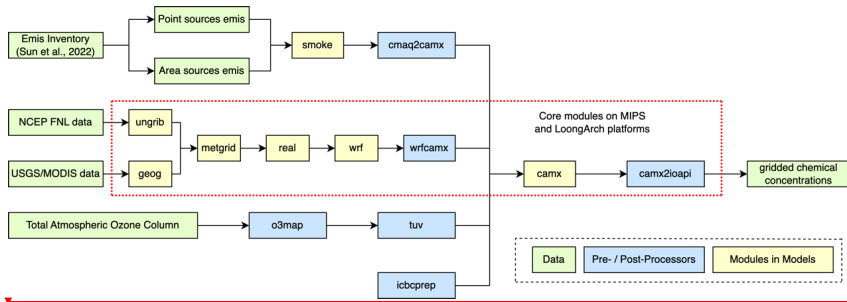
Deleted: platform

Deleted: both

Deleted:

Deleted: CPU

Deleted: and benchmark platform



135

136 **Figure 1.** Framework of WRF-CAMx modeling system. The core modules have been
 137 ported to MIPS and LoongArch CPU platforms. The core modules are framed by red
 138 dashed line in the figure.

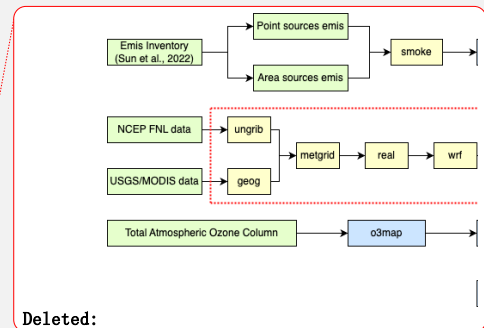
139 In Xi'an, China and Milan, Italy, the WRF-CAMx modelling system was applied,
 140 enabling high-resolution hourly model output of pollutant concentration within specific
 141 local urban areas (Pepe et al., 2016; Yang et al., 2020). The modeling system is widely
 142 used to study the spatial-temporal variation of pollutant concentration and source
 143 apportionment, analyze the contribution of regional transport to pollution and
 144 investigate the impact of initial conditions and emissions on pollution simulation in key
 145 regions such as the North China Plain, Sichuan Basin, and Fenwei Plain (Bai et al.,
 146 2021; Zhen et al., 2023; Zhang et al., 2022; Xiao et al., 2021).

147

148 2.1 Description of WRF-CAMx modeling system

149 WRF and CAMx serve as the core components of the modeling system. WRF is a
 150 mesoscale numerical weather prediction system designed for atmospheric research and
 151 operational forecasting applications. Distinguished by its high temporal and spatial
 152 resolution, WRF is suitable for multi-scale simulations of short-term weather forecast,
 153 atmospheric process, and long-term climate, making it an essential tool in the
 154 meteorological and atmospheric research communities (Powers et al., 2017). In the
 155 modeling system, WRF provided gridded meteorological field data for air quality
 156 model CAMx. The relative humidity, a meteorological variable used in result validation
 157 is calculated using the wrf-python package (Official website: [https://wrf-](https://wrf-python.readthedocs.io)
 158 [python.readthedocs.io](https://wrf-python.readthedocs.io), last access: October 2023). CAMx is an atmospheric pollutant

158



Deleted:

Deleted: '

Deleted: Europe

Deleted: developed

Deleted: WRF is a high-resolution mesoscale model, which can be utilized for various purposes such as weather research and forecasting, physical parameterization scheme research, data assimilation and mesoscale climate simulation.

Moved (insertion) [2]

Deleted: Relative humidity

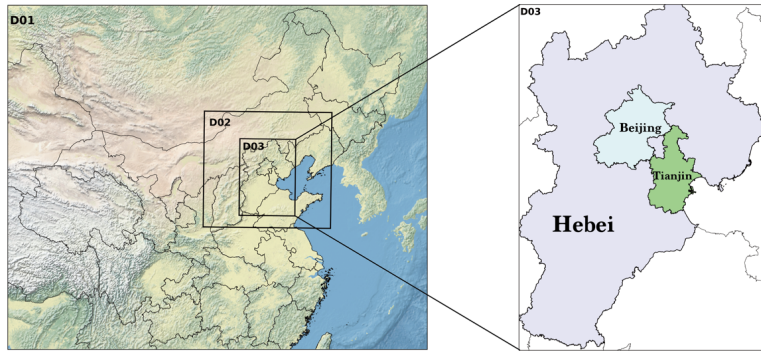
168 calculation model, which can be utilized for simulating and predicting the
169 concentrations of various air pollutants. The WRF and CAMx models are distinguished
170 by modularity and parallelism, using MPI in parallel computing, making them efficient
171 (Skamarock et al., 2019; RAMBOLL ENVIRON Inc., 2014).

172 In the modeling system, the SMOKE model and cmaq2camx program are used to
173 process emission data and provide model-ready gridded emission data for the CAMx
174 model. The wrfcamx program converts the WRF results into meteorological input files
175 which are compatible with CAMx. TUV is a radiation transfer model capable of
176 producing clean sky photolysis rate input files for the chemical mechanisms in CAMx,
177 and the o3map program prepares ozone column input files for TUV and CAMx. The
178 icbcprep program prepares initial and boundary condition files for CAMx with the
179 profile, and the effects of initial conditions have been studied by Xiao et al. (2021). The
180 camx2ioapi program converts the CAMx output files into netCDF format following the
181 Models-3/IO-API convention, and then uses NCL or other softwares to analyses the
182 model results.

183

184 **2.1.1 Model domain setup**

185 The model domain focusing on the Beijing-Tianjin-Hebei region has been set up
186 in this study. The WRF model has three nested domains with horizontal resolutions of
187 27km (D1), 9km (D2), and 3km (D3), as shown in Figure 2. The outer domain (D1)
188 covers most parts of China, and the inner domain (D3) covers Beijing, Tianjin, and
189 Hebei Province. The model domain is centered at (35°N, 110°E), with two true latitudes
190 located at 20°N and 50°N. The vertical resolution of WRF is 34 vertical layers. The
191 CAMx model has only one model domain, which is the innermost grid with a resolution
192 of 3km (D3), mainly covering the Beijing-Tianjin-Hebei region. The vertical resolution
193 of CAMx is 14 vertical layers, which is extracted from the WRF output files using the
194 wrfcamx module, and the lower seven layers of CAMx are same as those in the WRF
195 model.



196
197 **Figure 2.** The domains of three-level nested grids in the WRF-CAMx modelling system.
198 The respective horizontal resolutions are 27 km × 27 km (D1), 9 km × 9 km (D2), and
199 3 km × 3 km (D3).

200
201 **2.1.2 Model configuration**

202 Starting from 00:00 on November 3, 2020, until 24:00 on November 5, 2020, the
203 modelling system simulated the meteorological and air quality for a period of 72 hours.
204 In the research of Wang et al. in 2019, a 72h test case was set for the scientific validation
205 and performance evaluation of the chemistry transport models. A 72h case represents a
206 moderate-sized real scientific workload, which allows for simulating in a short time to
207 validate the results and assess computational efficiency on the MIPS and LoongArch
208 platforms. For the meteorological model, the global meteorological initial and boundary
209 fields for the WRF model are derived from the NCEP Global Final Reanalysis Data
210 (FNL), with a spatial resolution of 0.5° x 0.5° and a temporal resolution of 6 hours. And
211 the parameterization schemes of the WRF model used in the simulation case are shown
212 in Table 1.

213 For the air quality model, the meteorological files are provided by the WRF model
214 are used for the chemical transport module in CAMx. The emission inventory used in
215 the simulation case was obtained from Sun et al. (2022a). It contains basic emissions
216 from Sun et al. (2022b) and fugitive dust emission from bare ground surfaces. The
217 SMOKE model (v2.4) is used to process the emission inventory and provide gridded

Moved (insertion) [1]

Deleted: ,

Deleted: testing

Deleted: , and

Deleted: validating

Deleted: of the WRF-CAMx model on the MIPS platform

Deleted: assessing

emissions for CAMx. The parameterization schemes of the CAMx model used in the simulation case are shown in Table 2.

226

227 **Table 1.** Parameterization schemes of WRF in research case.

Parameterization process	Scheme
Microphysics	WSM3
Longwave radiation	RRTM
Shortwave radiation	Dudhia
Land surface	Noah
Planetary boundary layer	YSU
Cumulus parameterization	Kain-Fritsch(new Eta)

228

229 **Table 2.** Parameterization schemes of CAMx in research case.

Parameterization process	Scheme
Horizontal Diffusion	PPM
Vertical Diffusion	K-theory
Dry Deposition	Zhang03
Gas-phase chemical mechanism	CB05
Aqueous aerosol chemistry	RADM-AQ
Inorganic gas-aerosol partitioning	ISORROPIA

230

231 **2.1.3 Statistical indicators for model results**

232 To quantify the differences in the model results between the MIPS and benchmark
 233 platform, three statistical indicators are used to analyze the differences of concentration
 234 time series: Mean Absolute Error (MAE), Root Mean Square Error (RMSE), and Mean
 235 Absolute Percentage Error (MAPE). The MAPE quantifies the deviation between
 236 computational differences and simulated values. The smaller these indicators, the better
 237 accuracy and stability of scientific computing of the modeling system on the MIPS
 238 platform. The calculation formulas for these statistical indicators are provided in
 239 equations (1) to (3).

240
$$MAE = \frac{1}{n} \sum_{i=1}^n |MIPS(i) - Base(i)| \quad (1)$$

241
$$RMSE = \left[\frac{1}{n} \sum_{i=1}^n (MIPS(i) - Base(i))^2 \right]^{\frac{1}{2}} \quad (2)$$

242
$$MAPE = \frac{1}{n} \sum_{i=1}^n \left| \frac{MIPS(i) - Base(i)}{MIPS(i)} \right| \times 100\% \quad (3)$$

Moved (insertion) [3]

243 In the equations, n represents the number of grids in the domain. $MIPS(i)$ represents the
244 simulated value of a certain grid on the MIPS platform, and $Base(i)$ represents the
245 baseline value of a certain grid on the benchmark platform.

247 **2.2 MIPS and LoongArch CPU platforms description**

248 Loongson CPU platform was chosen for the porting work in the study. Currently,
249 the Loongson processor family has three generations of CPU products, evolving from
250 single-core to multi-cores architectures and from experimental prototypes to mass-
251 produced industrial products (Hu et al., 2011). The Loongson-2 processor is a 64-bit
252 general-purpose RISC processor series which is compatible with MIPS instruction set.
253 It can be used in personal computers, mobile terminals, and various embedded
254 applications, running many operating systems such as Linux and Android smoothly
255 (Zhi et al., 2012). Wu et al. (2019) reports the application of the mesoscale model on
256 Loongson 2F CPU platform. The Loongson-3 processor features a scalable multi-core
257 architecture, targeting high-throughput data centers, high-performance scientific
258 computing, and other applications, with the significant advantage of achieving a high
259 peak performance-to-power ratio and striking a well-balanced trade-off between
260 performance and power consumption (Hu et al., 2009).

261 The Loongson 3A series are multi-core processors designed for high-performance
262 computers, featuring with high bandwidth, and low power consumption. The efficient
263 design solution and the advantage of high energy efficiency ratio make servers based
264 on Loongson CPUs highly competitive in performance, power consumption, and cost-
265 effectiveness (Li et al., 2014; Wang et al., 2014). In this study, the Loongson platform
266 uses the Debian Linux operating system, commercially known as Tongxin UOS
267 (<https://www.uniontech.com>, last access: [January, 2024](#)), and the Loongson 3A4000
268 processor, which is the first quad-core processor based on GS464v 64-bit
269 microarchitecture in Loongson 3 Processor Family. The main technical parameters of
270 Loongson 3A4000 CPU are shown in Table 3. Compared to previously released CPUs,
271 the processor improves frequency and performance by optimizing on-chip interconnect
272 and memory access path, integrating 64-bit DDR4 memory controller and on-chip

Deleted: ¶

A lot of porting and optimization research work has been conducted to ensure the proper functioning of the high-performance mathematical library on Loongson platforms, resulting in improved computing performance, such as FFT (Fast Fourier Transform) (Guo et al., 2012; Li et al., 2011; Zhao et al., 2012). The porting and optimization efforts conducted on the multi-core Loongson processors have successfully demonstrated the stability and efficiency in the numerical computing applications. These results provide valuable technical references and rationality validation for the numerical model application on Loongson platform.

Deleted: October 2023

286 security mechanism. The Loongson 3A6000 CPU platform uses Loongnix, the open-
 287 source community edition operating system released by Loongson
 288 (<https://www.loongson.cn/system/loongnix>, last access: January, 2024), and the latest
 289 released Loongson 3A46000 processor, which is a quad-core processor based on LA664
 290 microarchitecture. The main technical parameters of Loongson 3A6000 CPU are shown
 291 in Table 3. The processor supports the LoongArch™ instruction set and hyper-threading,
 292 and the performance has significantly improved compared to the previously released
 293 processors (Hu et al., 2022).

294

295 **Table 3.** Main Parameters of Loongson 3A4000 CPU and Loongson 3A6000 CPU*

<u>Main Parameters</u>	<u>Loongson 3A4000 CPU</u>	<u>Loongson 3A6000 CPU</u>
<u>Main Frequency</u>	<u>1.8GHz–2.0GHz</u>	<u>2.0GHz–2.5GHz</u>
<u>Peak Computing Speed</u>	<u>128Gflops@2.0GHz</u>	<u>240Gflops</u>
<u>Transistor Technology</u>	<u>28nm</u>	<u>12nm</u>
<u>Number of Cores</u>	<u>4</u>	<u>4(Physical) 8(Logical)</u>
<u>Processor Cores</u>	<u>MIPS64 compatible Support 128/256-bit vector instructions</u>	<u>support LoongArch™ Support 128/256-bit vector instructions</u>
<u>High-speed I/O</u>	<u>2 x 16-bit HyperTransport 3.0 control</u>	<u>1 x HyperTransport 3.0 control</u>
<u>Typical Power Consumption</u>	<u><30W@1.5GHz <40W@1.8GHz <50W@2.0GHz</u>	<u>38W@2.5GHz</u>

296 *source: <https://www.loongson.cn>, last access: January, 2024,

297

298 **2.3 Benchmark platform description**

299 This study uses an X86 CPU platform as benchmark platform compared to the
 300 MIPS and LoongArch CPU platforms. The benchmark platform is powered by Intel
 301 Xeon E5-2697 v4 CPU, with strong floating-point performance and many technical
 302 features such as Intel Turbo Boost Technology (Intel Inc., 2023). The Intel Xeon E5-
 303 2697 v4 CPU has 18 cores, with 2.3GHz base frequency and 3.6GHz maximum Turbo
 304 Boost frequency, 45 MB Intel Smart Cache and 145W design power consumption. The
 305 operating system is CentOS Linux 7.4.1708. The main information for all platforms is

Deleted: <https://www>
 Formatted: Default Paragraph Font, Font: (Default) +Body (DengXian), 10.5 pt

Deleted:
 Deleted: Loogson 3A4000 CPU

Deleted: Loongson 3A4000 CPU Main Parameters
 Deleted: October 2023

Deleted: CPU platform

Deleted: both

313 shown in Table 4.

314

315 **Table 4.** The comparison of main configuration between MIPS, LoongArch and X86
316 platforms.

	<u>MIPS Platform</u>	<u>LoongArch</u> <u>Platform</u>	<u>X86 platform</u>
<u>CPU</u>	Loongson 3A4000	Loongson 3A6000	Intel Xeon E5-2697 v4
<u>Number of CPUs</u>	1	1	1
<u>Number of CPU cores</u>	4	8	18
<u>CPU Frequency</u>	1.8GHz	2.0Ghz	2.3GHz
<u>CPU instruction set</u>	MIPS64	LoongArch™	X86_64
<u>Operating system</u>	Tongxin UOS	Loongnix	CentOS Linux 7.4.1708
<u>Operating system kernel (Linux version)</u>	4.19.0-loongson-3- desktop	4.19.0-19- loongson-3	3.10.0- 957.1.3.el7.x86_64

317

318

319 2.4 The difference between MIPS, LoongArch and X86 platforms

320 In this study, the numerical model's source code is written in Fortran, and
321 commonly used compilers for X86 architecture include Intel Compiler, PGI and GNU
322 Compiler. The compiler for MIPS platform is built using GCC 8.3 MIPS GNU/Linux
323 cross-toolchain based on the open-source GNU Project, called MIPS GNU, and the
324 latest version is 8.3. And the compiler for LoongArch platform is built using GCC 8.3
325 LoongArch GNU/Linux cross-toolchain based on the open-source GNU Project, called
326 LoongArch GNU, and the latest version is 8.3. The compiler for the benchmark
327 platform is set to X86 GNU, and the version is also 8.3. Table 5 shows the differences
328 between all platforms' GNU compilers in terms of applicable platforms. Compared to
329 X86 GNU, the default compilation options of MIPS GNU compiler not only specify
330 the platform architecture but also include additional instruction sets, such as atomic

330

Formatted: Centered

Formatted: Centered

Formatted: Centered

Formatted: Centered

Formatted: Centered

Formatted: Centered

Formatted: Centered

Formatted: Centered

Deleted: ¶
MIPS Platform

Deleted: the two

Deleted: '

335 operation instruction set LLSC, shared library instruction set PLT, etc., which can
 336 optimize target programs compiled by GNU for MIPS architecture and improve
 337 computational efficiency. And the default compilation options of LoongArch GNU
 338 compiler not only specify the platform architecture but also include target
 339 microarchitecture tuning option, which can also optimize target programs compiled by
 340 GNU for LoongArch architecture.

341 **Table 5.** Comparison of GNU compiler between MIPS, LoongArch and X86 CPU
 342 platforms.

<u>Artitecture</u>	<u>MIPS64</u>	<u>LoongArch</u>	<u>x86_64</u>
<u>Compiler</u>	MIPS GNU Fortran	LoongArch GNU Fortran	X86 GNU Fortran
<u>Version</u>	8.3	8.3	8.3
<u>Target</u>	mips64el-linux-gnuabi64	loongarch64-linux-gnu	x86_64-redhat-linux
<u>Options (Architecture)</u>	-march=mips64r2 -mabi=64	-march=loongarch64 -mabi=lp64d	-march=x86-64 -mtune=generic
<u>Options (Instruction set)</u>	-mllsc -mplt - mmadd4	-mtune=loongarch64	/
<u>FLAGS(WRF)</u>	-fconvert=big-endian -frecord-marker=4 -ffree-line-length-none -O2 -fvectorize -funroll-loops		
<u>FLAGS(CAMx)</u>	-fconvert=big-endian -frecord-marker=4 -ffixed-line-length-none -fno-align-commons -O2		

343 The WRF-CAMx modeling system depends on several scientific computing
 344 libraries. Firstly, the general data format libraries netCDF and HDF5 are required to
 345 store the large-scale gridded data for the modeling system. NetCDF is a self-describing
 346 data format developed by NCAR/Unidata, primarily used for storing multidimensional
 347 array data in fields like meteorology and earth sciences (UCAR/Unidata, 2021). HDF5
 348 is a data format developed by HDF GROUP that supports complex data structures with
 349 multiple data types and multi-dimensional datasets (The HDF Group, 2019). In this
 350 study, netCDF-C (v4.8.1), netCDF-Fortran (v4.5.3), HDF5 (v1.12.1) and IOAPI (v3.1)
 351 were successfully installed on MIPS and LoongArch platforms by building from their
 352 sources, which are obtained from the official website.

353 The MPICH library is required to support parallel computing in the modeling
 354 system. In order to fully utilize computing resources, the method of MPI message

Deleted: Artitecture ... 13

356 communication is used in WRF and CAMx model (Wu et al., 2012). MPICH is an
357 open-source, portable parallel computing library for implementing the MPI standard
358 (Amer et al., 2021). It supports inter-process communication and data exchange in the
359 parallel computing environment. Similarly, this study successfully installed MPICH
360 (v3.4) on MIPS [and LoongArch](#) platforms by building from its source. During the
361 compilation and installation of the mentioned libraries above, the configure tool was
362 used to check the basic information of the platform's CPU and compiler, and prepare
363 for compatibility with platform before compilation, the GNU compiler is used to
364 compile the source code of libraries, and the cmake tool is used to install the libraries.
365 Additionally, the same runtime environment as MIPS platform was also built on the
366 benchmark platform.

367

368 **3 Porting the WRF-CAMx modelling system on MIPS [and LoongArch](#)** 369 **CPU platforms**

370 The simulation result is influenced by several factors including processor
371 architecture, operating system, compiler, parallel environment, and scientific
372 computing libraries. In order to ensure stability and accuracy of numerical simulation,
373 the models should be adapted to the new runtime environment when porting across
374 platforms. Additionally, various operating systems have different tools, software and
375 libraries, which may impact the results of numerical simulations.

376 In this study, the runtime environment for WRF-CAMx modeling system was built
377 on MIPS [and LoongArch](#) platforms, [including parallel computing libraries such as](#)
378 [MPICH3 \(v3.4\) and data format libraries such as HDF5 \(v1.15.1\) and NETCDF \(C-](#)
379 [v4.8.1, Fortran-v4.5.3\)](#). [These libraries do not support the architecture \(mips64el and](#)
380 [LoongArch\) and GNU compiler of Loongson platform. Relevant information needs to](#)
381 [be added to the free software config.guess and config.sub provided by GNU org. Part](#)
382 [of the information is shown in subfigure a\) in Figure 3, which can help identify the](#)
383 [platform architecture and system during the compilation and installation of libraries](#)
384 [using Configure and Make tools.](#) The configuration files for making the models were

385 modified to fit the compilers of the Linux system on MIPS and LoongArch platforms.

386 In order to verify the stability of scientific computing on MIPS and LoongArch
387 platforms, a control experiment was set up on the benchmark platform, minimizing the
388 impact of other factors on simulation results of both platforms.

389 The WRF v4.0 and CAMx v6.10 were successfully deployed on MIPS and
390 LoongArch platforms through source code compilation and installation. In the WRF
391 model, the default options for GNU compiler which are suitable for MIPS and
392 LoongArch architecture CPUs are not provided in the configure file of the source code
393 package, and it is necessary to incorporate architecture-specific settings for the model.
394 For example, the architecture presets are stored in the configure.defaults file, but
395 settings about the Loongson platform is not included. Specific architecture details,
396 including CPU architecture, GNU compiler and compilation flags, need to be added,
397 which can ensure the correct display of configuration during building WRF model, and
398 part of information is shown in subfigure b) in Figure 3. Table 5 provides the detailed
399 information added in the configure file, mainly about MIPS and LoongArch GNU
400 Fortran. When compiling Fortran programs on MIPS and LoongArch platforms, the
401 MIPS and LoongArch GNU Fortran and necessary compilation flags must be specified.
402 These flags include common Fortran file format flags such as -fconvert=big-endian and
403 -frecord-marker=4, as well as optimization flags such as -O2 -ftee-vectorize -funroll-
404 loops. By specifying the appropriate compiler and flags for MIPS and LoongArch
405 architectures, the configure tool will provide necessary settings to compile WRF.
406 Correspondingly, when compiling WRF on the benchmark platform, the compilation
407 flags are strictly consistent with those of MIPS and LoongArch CPU platforms, which
408 ensures that differences in simulation results of two platforms are primarily attributed
409 to the underlying hardware architecture rather than changes in compilation settings.

410 In the CAMx model, the makefile provides information about parallelism and
411 compilers. Similarly, information about the CPU architecture, GNU compiler, and
412 compilation flags on MIPS and LoongArch platforms also needs to be added in the
413 makefile. For the detailed information added in the makefile, please refer to Table 5.
414 Additionally, the code of CAMx was modified to make it run smoothly on MIPS and

Deleted: UOS

Deleted: manually add information about the CPU architecture, GNU compiler, and compilation flags on MIPS platform...

419 LoongArch platform. Taking some function in the CAMx model for example, the model
420 frequently uses the “write” function for formatted output. The format specifiers in the
421 parameters consist of data types (I, F, E, A, X, etc.) followed by a character width. In
422 the CAMx model, the format specifiers in the write function mostly default to character
423 width, but there is a compilation issue with MIPS GNU, requiring character width
424 descriptors. It is also essential to ensure consistency with the default precision. A
425 specific example is illustrated in the figure below. A specific example is showed in in
426 subfigure c) in Figure 3. So far, the WRF-CAMx model has been successfully compiled
427 and installed on the MIPS and LoongArch platforms after modifications of the
428 configuration files mentioned above.

a)

```

''
loongarch32:Linux:*:* | loongarch64:Linux:*:*
GUESS=$UNAME_MACHINE-unknown-linux-$LIBC
;;
''
mips64el:Linux:*:*
GUESS=$UNAME_MACHINE-unknown-linux-$LIBC
;;

```

b)

```

#ARCH Linux mips64 gfortran compiler with gcc #serial smpar dmpar dm+sm
#
DESCRIPTION = GNU ($SFC/$SCC)
DMPARALLEL = # 1
DMPCPP = # -D_OPENMP
DMP = # -fopenmp
DMPCC = # -fopenmp
SFC = gfortran
SCC = gcc
CCOMP = gcc
DM_FC = mpif90 -f90-$(SFC)
DM_CC = mpicc -cc-$(SCC)
FC = CONFIGURE_FC
CC = CONFIGURE_CC
LD = $(FC)
RWORDSIZE = CONFIGURE_RWORDSIZE
PROMOTION = #-fdefault-real-8
ARCH_LOCAL = -DNONSTANDARD_SYSTEM_SUBR -DWRF_USE_CLM
CFLAGS_LOCAL = -w -O3 -c
LDFLAGS_LOCAL
CPLUSPLUSLIB = $(CPLUSPLUSLIB)
ESMF_LDFLAG =
FCOPTIM = -O2 -ffree-vectorize -funroll-loops
FCREDUCEDOPT = $(FCOPTIM)
FCNOOPT = -O0

```

c)

```

Before modification:
write (iout,'(a,2a)' ' spec','total [ug/m3]','c* [ug/m3] '
write (iout,'(i5,2e)') (idx(i),sctot(i),scsat(i),i=1,nsol)
write (iout,'(a,2e)' ' cpre,cpx ' ,cpre,cpx
After modification:
write (iout,'(a5,2a15)' ' spec','total [ug/m3]','c* [ug/m3] '
write (iout,'(i5,2e15.7)') (idx(i),sctot(i),scsat(i),i=1,nsol)
write (iout,'(a5,2e15.7)' ' cpre,cpx ' ,cpre,cpx

```

429

430 [Figure 3. Sample codes containing configure index, architecture-specific settings and](#)
431 [functions in the WRF-CAMx model. Panel a\) provides architecture information for](#)
432 [configuration. Panel b\) shows architecture-specific settings for WRF. Panel c\)](#)
433 [illustrates the sample code of functions in the CAMx before and after modification.](#)

434 4 The differences of model results on the two platforms

435 4.1 Validation of the spatial distribution

436 A [72h](#) simulation case has been designed to test the stability and availability of the
437 WRF-CAMx modeling system on the MIPS CPU platform in Beijing. By analyzing the
438 differences in simulation results and computing time, the accuracy and performance of

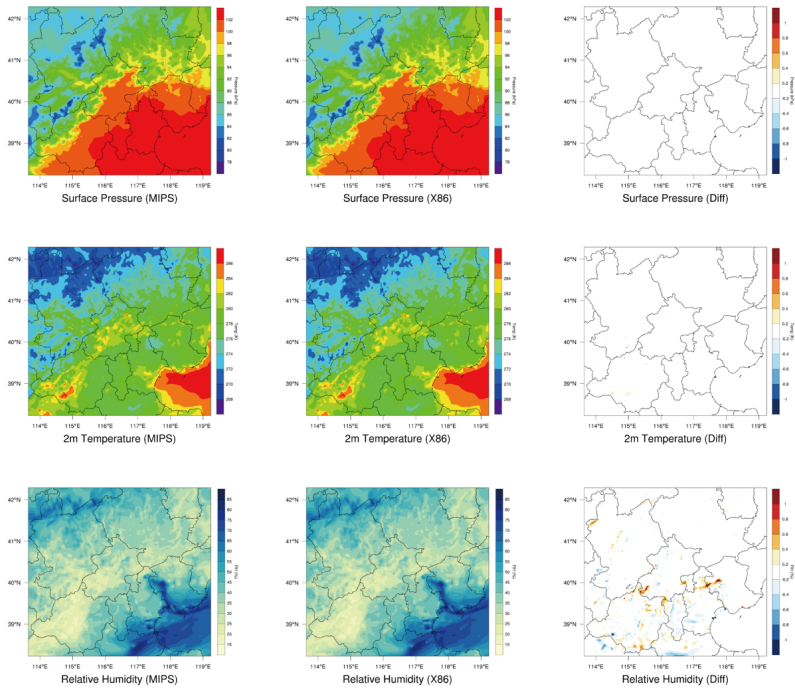
Moved up [1]: Starting from 00:00 on November 3, 2020, until 24:00 on November 5, 2020, the modelling system simulated the meteorological and air quality for a period of 72 hours, represents a moderate-sized real scientific workload, which allows for testing in a short time, and validating the results of the WRF-CAMx model on the MIPS platform and assessing computational efficiency.

446 the modeling system on MIPS platform were evaluated, which further verifies the
 447 feasibility and stability of the modeling system after porting to the MIPS platform.

448 Common meteorological variables, including 2-meter temperature, land surface
 449 pressure, and relative humidity were selected to verify the WRF model results. Figure
 450 4 shows the spatial distribution of the four meteorological variables after 72 hours
 451 simulation on different platforms, as well as the absolute errors (AEs). The
 452 meteorological variables from the modeling system on the different platforms exhibit a
 453 generally consistent spatial distribution in the Beijing-Tianjin-Hebei regions shown in
 454 Figure 4.

Deleted: 3

Deleted: 3



455
 456 **Figure 4.** Spatial distribution of 2m temperature, surface pressure, relative humidity
 457 from WRF. Left column, MIPS platform. Middle, the X86 platform. Right, the
 458 differences between the MIPS and benchmark(X86) platform. ▲

Deleted: 3

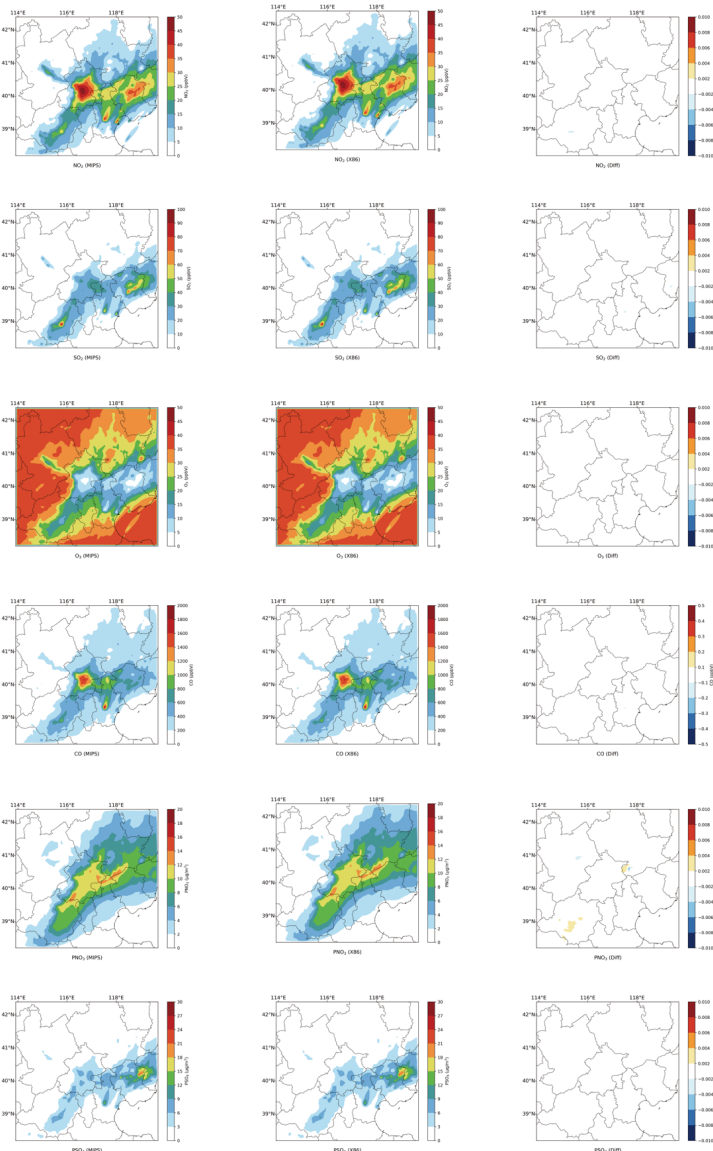
459
 460 Similarly, the NO₂, SO₂, O₃, CO, PNO₃ and PSO₄ were selected to verify the

Moved up [2]: Relative humidity is calculated using the wrf-python package (Official website: <https://wrf-python.readthedocs.io>, last access: October 2023).

467 CAMx model results on the MIPS platform. Figure 5 shows the spatial distribution of
468 the six species, as well as the absolute errors (AEs) between the two platforms after 72
469 hours simulation. Simulating the 72h-case with four parallel processes using MPICH,
470 CAMx takes about 9h on Loongson 3A4000 CPU and 2.6h on Intel Xeon E5-2697 v4
471 CPU. As shown in Figure 5, the spatial distribution of air pollution concentrations from
472 the different platforms is essentially consistent, appearing very similar visually.

Deleted: 4

Deleted: 4



475

476 **Figure 5.** Spatial distribution of NO₂, SO₂, O₃, CO, PNO₃ and PSO₄ from CAMx on
 477 MIPS and benchmark platform. Left column, MIPS platform. Middle, the X86 platform.
 478 Right, the differences between the MIPS and benchmark(X86) platform.

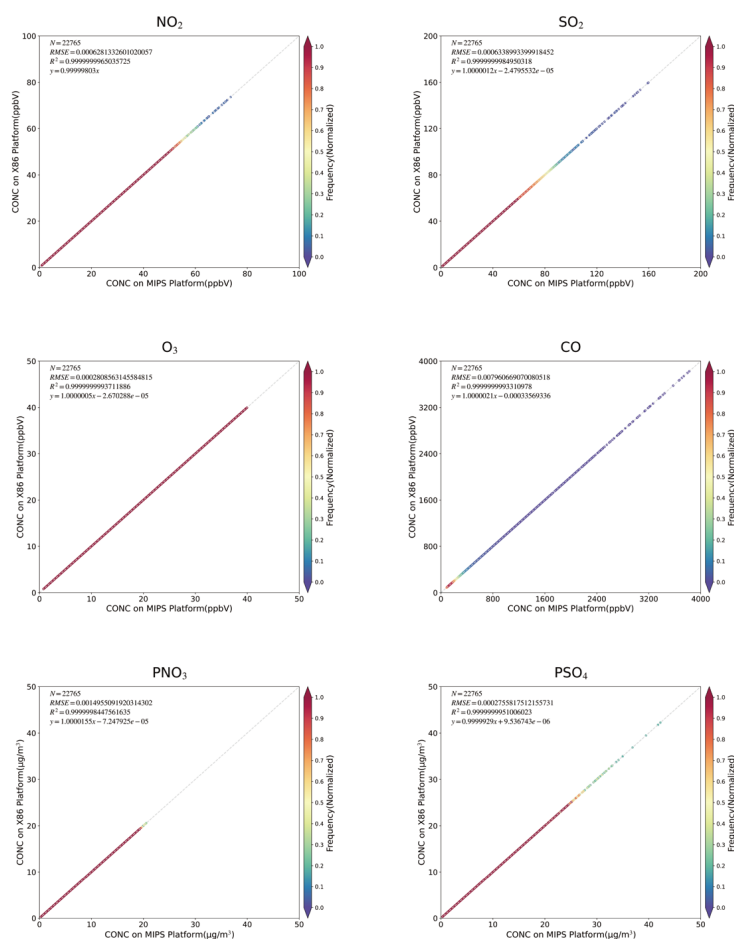
Deleted: 4

479

As shown in Figure 6, the scatter plots between the two platform, it can be seen

Deleted: 5

482 that for the total of 22,765 grids within the 145x157 simulation domain, the root mean
 483 square errors (RMSEs) of the six species between the MIPS platform and benchmark
 484 platform are close to 0.001, which is essentially 0. The linear regression model was
 485 used to fit the scatters, and the regression slopes for each species are nearly 1, with
 486 intercepts close to 0, and the R2 values used for the goodness of fit are nearly 1. The
 487 fitted lines closely coincide with the “y=x” line, indicating that the differences between
 488 the MIPS and X86 platform for each species are minimal to negligible.



489
 490 **Figure 6.** Scatter of grid concentrations for NO₂, SO₂, O₃, CO, PNO₃ and PSO₄ from
 491 CAMx on the MIPS and benchmark platform. The density of scatters is represented by

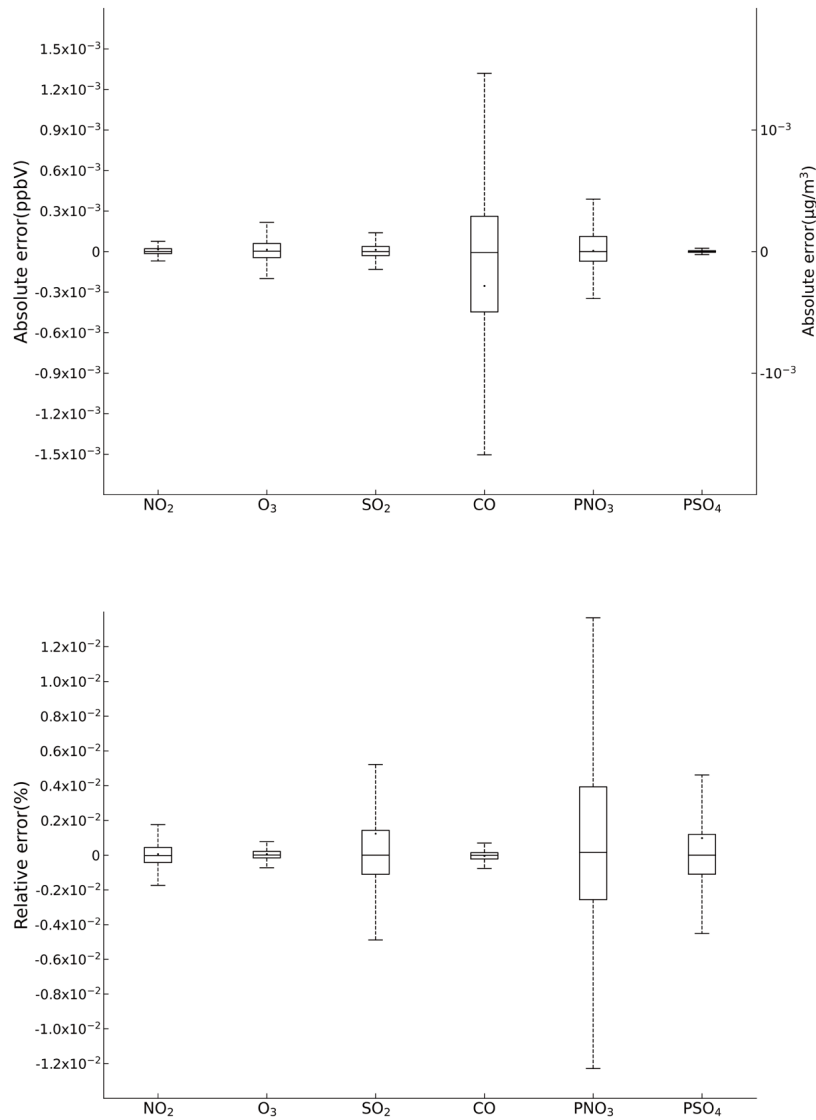
Deleted: 5

493 the colors.

494 Figure 7 is the boxplots which show the absolute errors (AE) and relative errors
495 (RE) of the six species between MIPS and benchmark platform. According to Figure 7,
496 the absolute errors of the six species are generally in the range of $\pm 10^{-3}$ ppbv (parts per
497 billion by volume; the unit of NO₂, SO₂, O₃ and CO concentration) or $\mu\text{g m}^{-3}$ (the unit
498 of particle composition PNO₃ and PSO₄), and the relative errors are generally in the
499 range of $\pm 0.01\%$. Specially for CO, it exhibits more pronounced AEs compared to other
500 species. In some grid boxes, the AEs between MIPS and benchmark platform exceed
501 the range of $\pm 10^{-3}$ ppbv, but they remain in the range of $\pm 10^{-2}$ ppbv. In summary, there
502 are some errors between the results of the modeling system on the MIPS and benchmark
503 platform during the porting process. However, these errors are relatively minor
504 compared to the numerical values. The reasons are attributed to the differences in the
505 CPU architecture and compiler characteristics between the two platforms, such as data
506 operations and precision running on different CPUs, which are primarily responsible
507 for the observed errors.

Deleted: 6

Deleted: 6



510

511 **Figure 7.** The absolute errors and relative errors for NO₂, SO₂, O₃, CO, PNO₃ and PSO₄
 512 concentration in all grids between the MIPS and benchmark platform.

Deleted: 6

513 Additionally, random grids in the domain were selected to assess the precision of
 514 simulation results in localized regions. The positions of these grids were determined

516 based on 32 observation stations in Beijing, and the nearest grid was determined using
517 the Euclidean Shortest Distance in the domain. The station map is presented in Figure
518 S1 in the Supplement. The Taylor diagram is used to assess the precision of
519 concentrations for six species near the observation stations, and the scatters
520 representing the six species at 32 stations are highly overlapping. Statistical parameters
521 used in the Taylor diagram, such as the correlation coefficient (R) approaching 1,
522 normalized standard deviation (NSD) and normalized root mean square error (NRMSE)
523 approaching 0, indicate high precision of the simulation results at specific stations on
524 the MIPS platform.

525

526 **4.2 Validation of the temporal distribution from the two platform**

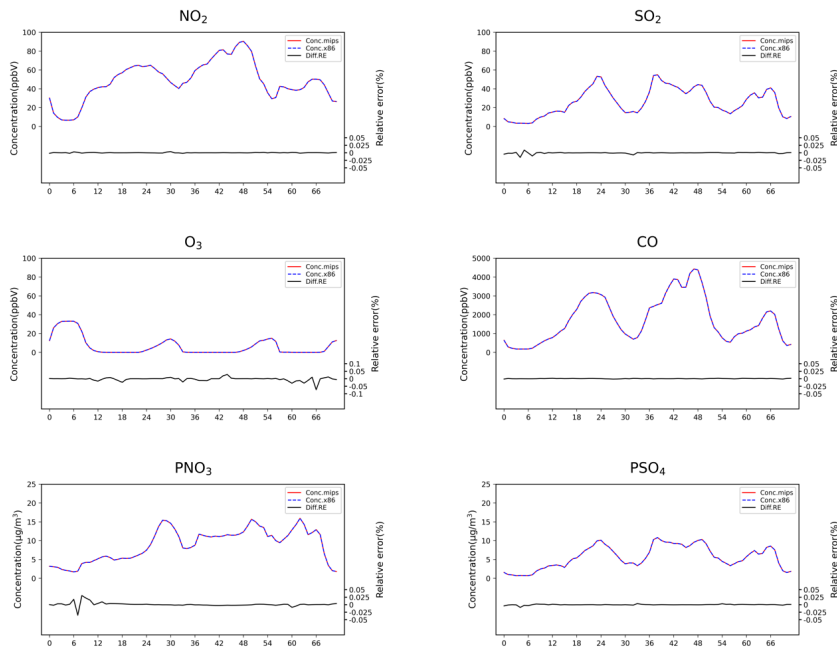
527 The time series of computational differences also be evaluated in this study.
528 Random grid in the domain was selected to examine the hourly concentrations of the
529 six species. Taking the example of the Beijing Olympic Center station (116.40°E,
530 39.99°N) from the National Standard Air Quality (NSAQ) stations, the time series of
531 hourly concentrations in the grid of the Beijing Olympic Center station and relative
532 errors between the MIPS and benchmark platform over the 72-hour period were shown
533 in Figure 8. As shown in Figure 8, it can be seen that the time series of the air pollutant
534 concentrations were highly consistent between the two platforms. In the 72-hour period,
535 the relative errors for NO₂, SO₂, CO and PSO₄ remain in ±0.025%. For PNO₃, the
536 relative errors remain in ±0.05%, and for O₃, they remain in ±0.1%. This indicates that
537 the errors caused by different architectures are within a reasonable range.

Deleted:

Deleted:

Deleted: 7

Deleted: 7



542
543 **Figure 8.** Time-series of NO₂, SO₂, O₃, CO, PNO₃ and PSO₄ concentrations and its
544 relative errors (RE) at the Beijing Olympic Sports Center site between the MIPS and
545 X86 platform. The red solid line and the blue dashed line, the CAMx model results on
546 MIPS platform and X86 platform. The black solid line shows the relative errors (RE)
547 between the MIPS and X86 platform.

548
549 **Figure 9** shows the time series of the concentration and their statistical indicators,
550 MAE, RMSE, and MAPE during the 72-hour simulation. As show in the figure, for
551 NO₂, SO₂, O₃, and PSO₄, the MAEs are all below 10⁻³ ppbv (µg m⁻³), and the RMSEs
552 are all below 10⁻³. The MAEs for CO and PNO₃ are below 10⁻² ppbv (µg m⁻³), and the
553 RMSEs for PNO₃ are below 10⁻², while the RMSEs for CO are below 10⁻¹. This is
554 because that PNO₃ and CO have relatively higher background concentrations compared
555 to the other species. The MAPE of PNO₃ concentration mainly ranging in 0-0.5%, while
556 the MAPE of CO concentration has the lowest values below 0.001%, and the other
557 species are in the range of 0-0.01%. Overall, the above time-series analysis verifies the
558 accuracy and stability of the modeling system on the MIPS platform.

Deleted: 7

Moved up [3]: To quantify the differences in the model results between the MIPS and benchmark platform, three statistical indicators are used to analyze the differences of concentration time series: Mean Absolute Error (MAE), Root Mean Square Error (RMSE), and Mean Absolute Percentage Error (MAPE). The MAPE quantifies the deviation between computational differences and simulated values. The smaller these indicators, the better accuracy and stability of scientific computing of the modeling system on the MIPS platform. The calculation formulas for these statistical indicators are provided in equations (1) to (3).¶

$$MAE = \frac{1}{n} \sum_{i=1}^n |MIPS(i) - Base(i)| \quad (1)¶$$

$$RMSE = \left[\frac{1}{n} \sum_{i=1}^n (MIPS(i) - Base(i))^2 \right]^{\frac{1}{2}} \quad (2)¶$$

$$MAPE = \frac{1}{n} \sum_{i=1}^n \left| \frac{MIPS(i) - Base(i)}{MIPS(i)} \right| \times 100\% \quad (3)¶$$

In the equations, n represents the number of grids in the

Deleted: $MAE = \frac{1}{n} \sum_{i=1}^n |MIPS(i) -$
(1)¶

$Base(i)|$
 $RMSE = \left[\frac{1}{n} \sum_{i=1}^n (MIPS(i) - Base(i))^2 \right]^{\frac{1}{2}} \dots$
(2)¶

$MAPE = \frac{1}{n} \sum_{i=1}^n \left| \frac{MIPS(i) - Base(i)}{MIPS(i)} \right| \times 100\% \dots$
(3)¶

Deleted: $RMSE = \left[\frac{1}{n} \sum_{i=1}^n (MIPS(i) - Base(i))^2 \right]^{\frac{1}{2}} \dots$
(2)¶

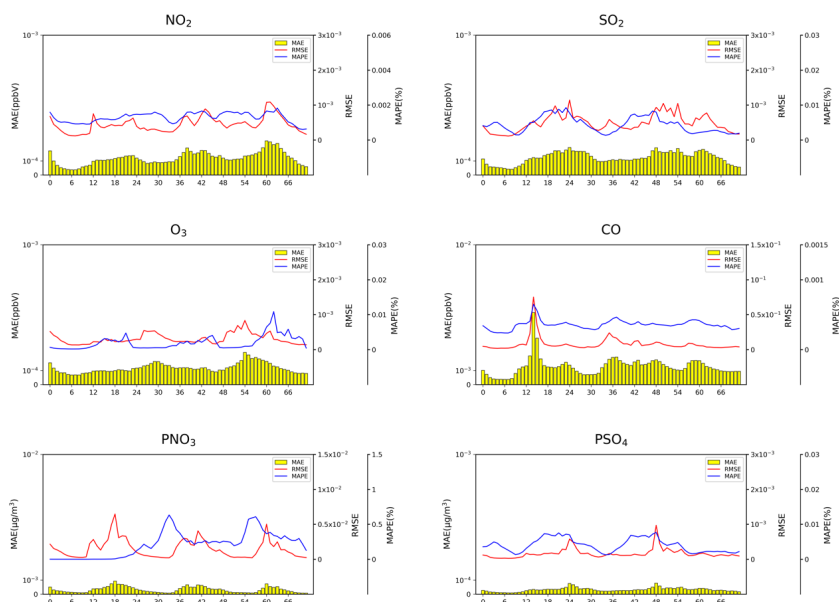
$MAPE = \frac{1}{n} \sum_{i=1}^n \left| \frac{MIPS(i) - Base(i)}{MIPS(i)} \right| \times 100\% \dots$
(3)¶

In the equations, n represents the number of grids in the

Deleted: $MAPE = \frac{1}{n} \sum_{i=1}^n \left| \frac{MIPS(i) - Base(i)}{MIPS(i)} \right| \times 100\% \dots$
(3)¶

In the equations, n represents the number of grids in the domain. $MIPS(i)$ represents the simulated value of a certain grid on the MIPS platform, and $Base(i)$ represents the baseline value of a certain grid on the benchmark platform.¶

Deleted: 8



634

635 **Figure 2.** Time series of MAEs, RMSEs and MAPEs for NO₂, SO₂, O₃, CO, PNO₃ and
 636 PSO₄ concentration in the 72h simulation. The yellow bar, the MAE. The red lines,
 637 RMSE, the blue lines, MAPE.

638

639 In this study, the evaluation method proposed by Wang et al. (2021) was also used
 640 to assess the scientific applicability of the model results on the MIPS platform. The
 641 Root Mean Square Errors (RMSEs) for NO₂, SO₂, O₃, CO, PNO₃ and PSO₄
 642 concentration between the MIPS and benchmark platform were computed, along with
 643 the standard deviations (stds) used to describe the spatial variation of species, and the
 644 ratio of RMSE to std, as shown in Table 6. The differences of the four species between
 645 the two platforms are negligible compared to their own spatial variations. Therefore,
 646 the results on the MIPS platform meet the accuracy requirements for research purpose.

647

648 **Table 6.** RMSE, std, RMSE/std for NO₂, SO₂, O₃, CO, PNO₃ and PSO₄.

	Differences in results	Spatial variation	RMSE/std
	RMSE	std	
NO ₂	6.3×10^{-7}	0.01	5.9×10^{-5}

Deleted: 8

O₃	2.8×10^{-7}	0.01	2.5×10^{-5}
SO₂	6.3×10^{-7}	0.02	3.9×10^{-5}
CO	7.9×10^{-6}	0.30	2.6×10^{-5}
PNO₃	1.5×10^{-3}	3.8	3.9×10^{-4}
PSO₄	2.7×10^{-4}	3.9	6.9×10^{-5}

650

651 In fact, the differences in model results cannot be completely eliminated, primarily
652 due to the varying CPU architectures and compilers. In the practical applications,
653 compared with the errors arising from the inherent uncertainties of the modeling system
654 and the input data, the differences of model results between different platforms can even
655 be considered negligible. The comprehensive analysis demonstrates that the results of
656 the WRF-CAMx modeling system on the MIPS CPU platform are reasonable.

657

658 **5 The evaluation about computational performance**

659 Scientific computing involves a significant amount of floating-point operations,
660 and the floating-point computational capability is a crucial indicator for CPU
661 performance. In this study, the simulation case was configured to conduct parallel
662 computing tests on the MIPS, [LoongArch](#) and benchmark platform. These tests
663 included assessing the CPU's single-core performance with the non-parallel model and
664 the platform's parallel performance with the parallel model using multiple processes.
665 The time of CAMx model running simulation case for [24](#) hours in the modeling system
666 are shown in Figure [10](#). From the figure, it can be observed that under single-core
667 conditions, the computing capability of the MIPS platform for CAMx is approximately
668 one-third of the X86 benchmark platform, [and the LoongArch platform is slightly lower](#)
669 [than the X86 benchmark platform.](#)

670 It's worth noting that the simulation time of the CAMx model for running with two
671 processes in parallel and running in non-parallel remains approximately consistent. This
672 is because the MPI used in CAMx is designed using a "master/slave" parallel processing
673 approach, and a process is allocated for input/output and message communication
674 during the runtime (Cao K et al., 2023). This process doesn't perform any simulation in
675 the model. Therefore, the time required for parallelism of two processes is comparable

Deleted: 2

Deleted: 9

678 to the non-parallelism, and in some cases, it might even be slightly longer due to the
679 overhead of MPI communication. Compared to non-parallel, the speedup of the MIPS
680 platform with four-process parallelism using MPICH3 is approximately 2.8, while
681 using OpenMP is about 2.9, and the speedup of the LoongArch platform with four-
682 process parallelism using MPICH3 is approximately 2.8, while using OpenMP is about
683 2.9. For the X86 benchmark platform, running with four processes in parallel using
684 MPICH3 has a speedup of approximately 2.7.

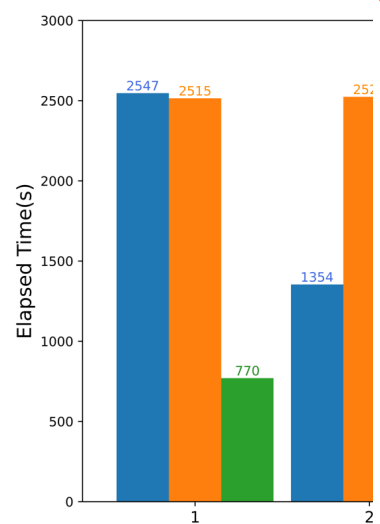
685 Additionally, the performance of the MIPS platform significantly decreases when
686 the number of parallel processes exceeds 4. This is because the modeling system
687 involves compute-intensive tasks. The Loongson 3A4000 CPU has four cores, and
688 when the number of processes called by MPI matches the number of CPU cores, the
689 CPU utilization can approach 100%. Further increasing the number of processes, the
690 cores will compete for CPU resources, resulting in additional overhead and reduced
691 computational efficiency. As for LoongArch platform, the performance slightly
692 decreases when the number of parallel processes exceeds 4. The Loongson 3A6000
693 CPU has four physical cores and eight logical cores, and when the number of processes
694 called by MPI matches the number of physical cores, the computational load is evenly
695 distributed across each core. Although the Loongson 3A6000 supports hyper-threading,
696 further increasing the number of processes, CPU starts to schedule logical cores to
697 allocate computational load. Thread scheduling will result in additional overhead and
698 reduced computational efficiency. This explains why the elapsed time is slightly higher
699 when CAMx running with 5 parallel processes compared to 4 parallel processes as
700 shown in the section 2 of Supplementary Material.

Deleted: .

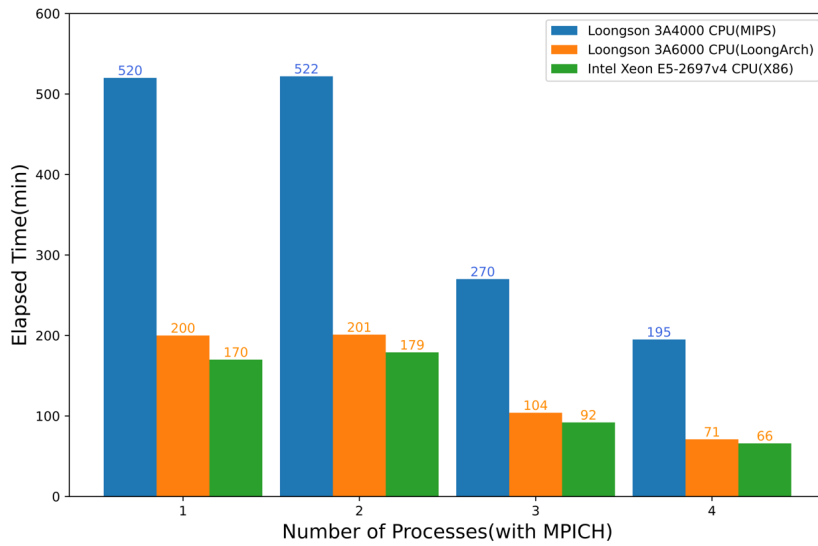
Formatted: Indent: First line: 2 ch

Deleted: reaches 5

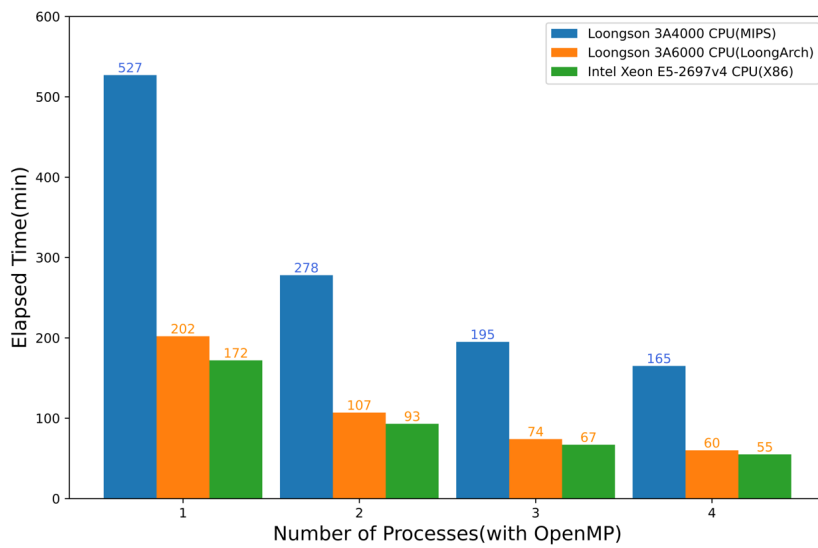
Deleted: ¶



Deleted:



705



706

707 **Figure 10.** Elapsed time of CAMx model running simulation case with MPICH and
 708 OpenMP for 24 hours on the MIPS, LoongArch and benchmark platforms.

Deleted: 9

Deleted: 2

709

710 In the recent years, the Loongson CPUs have been continuously upgraded.
 711 Compared to the previous generations of products, the performance of Loongson CPUs
 712 has shown significant improvement. Wu et al. (2019) simulated a nested domain

Deleted: the Loongson 3A4000 CPU

716 covering Beijing for 48 hours using the MM5 model on the Loongson 3A quad-core
717 CPU platform. The results showed that the computational capacity of the Loongson 3A
718 platform for the MM5 model is approximately equivalent to around 1/12 of the Intel
719 Core 2 Q8400 quad-core CPU, which was released in the same year. In the study of
720 Luo et al. (2011), a comparison between Loongson 3A and Intel i5 was made by running
721 NPB benchmark on each platform. The results shows that the performance of the 3A is
722 nearly one-tenth of that of the i5. The rapid development of Loongson CPUs has
723 provided a strong hardware foundation for the application of numerical simulation and
724 scientific computing on MIPS and LoongArch architecture CPU platforms. Based on
725 the performance evaluation of WRF-CAMx modeling system on Loongson 3A4000
726 and Loongson 3A6000 platform, it could be found that the computing capability nearly
727 tripled while maintaining similar power consumption. The adaptation and optimization
728 of the models based on RISC CPUs will also be an important research direction in the
729 future. Many factors influencing parallel performance, such as computing scale, I/O,
730 multiprocessor, etc., will be considered to evaluate on platforms with stronger
731 performance and more processors in the future.

Deleted: MIPS

732

733 6 Conclusion

734 This study describes the application of the WRF-CAMx model on the MIPS CPU
735 platform. The platform used in this study is Loongson 3A4000 quad-core CPU with the
736 main frequency of 1.8-2.0GHz, which can offer a peak operational speed of 128GFlops.

Deleted: 2.0GHz

Deleted: offering

737 It is equipped with the MIPS GNU compiler. The benchmark platform used the Intel
738 Xeon E5-2697 v4 CPU along with the same version of X86 GNU compiler. Based on
739 the characteristics of CPU architecture and compiler, this study has successfully
740 completed the construction of runtime environment for the WRF-CAMx modeling
741 system. The application of an air quality modelling system based on WRF-CAMx was
742 successfully tested using a 72-hour simulation case in the Beijing-Tianjin-Hebei region.

743 The results showed that the spatial distribution of the meteorological variables and
744 air pollutant species was nearly identical, with relative errors in the range of $\pm 0.1\%$.

748 Statistically, the maximum MAEs of major species ranged from 10^{-3} to 10^{-2} ppbv (μg
749 m^{-3}), the maximum RMSEs ranged from 10^{-2} to 10^{-1} ppbv ($\mu\text{g m}^{-3}$), and the MAPEs
750 remained within 0.5%, that the differences caused by the architectures and compilers
751 were within a reasonable range. Simulating a 2h-case with four parallel processes using
752 MPICH, CAMx takes about 15.2min on Loongson 3A4000 CPU and 4.8 min on Intel
753 Xeon E5-2697 v4 CPU. In terms of single-core CPU performance, the single-core
754 computing capability of Loongson 3A4000 CPU for the WRF-CAMx modeling system
755 is about one-third of Intel Xeon E5-2697 v4 CPU.

756 Currently, Loongson Technology has **focused on** the LoongArch architecture and
757 it has been used in the **latest** product. It is foreseeable that the LoongArch architecture
758 will lead to more significant performance improvements. In the future, as the numerical
759 models become more complex and computational scales become larger, more models
760 will be tested on high-performance computing platforms equipped with the LoongArch
761 architecture CPUs.

762

763 **Code and data availability.** The source codes of CAMx version 6.10 are available at
764 <https://camx-wp.azurewebsites.net/download/source> (ENVIRON, 2023). The datasets
765 related to this paper and the **binary executable files of CAMx for MIPS and LoongArch**
766 CPUs are available online via ZENODO (<https://doi.org/10.5281/zenodo.10722127>).

767

768 **Supplement.** The supplement related to this article is available on-line.

769

770 **Author contributions.** ZB and QW conducted the simulation and prepared the materials.
771 QW planned and organized the project. ZB and QW completed the porting and
772 application of the model for MIPS **and LoongArch** CPUs. YS collected and prepared
773 the emission data for the simulation. ZB, QW, KC, and HC participated in the
774 discussion.

775

776 **Acknowledgements.** The National Key R&D Program of China (2020YFA0607804)
777 and the Beijing Advanced Innovation Program for Land Surface funded this work. The

Deleted: introduced

Deleted: which is compatible with MIPS,

Deleted: next-generation

Deleted: , the 3A5000 CPU (Hu et al., 2022)

Deleted: CAMx codes

Deleted: <https://zenodo.org/records/10297970>

784 research is supported by the High Performance Scientific Computing Center (HSCC)
785 of Beijing Normal University.

786

787 **Competing interests.** The contact author has declared that none of the authors has any
788 competing interests.

789

790 **References**

- 791 Amer, A., Balaji, P., Bland, W., Gropp, W., Guo, Y., Latham, R., Lu, H., Oden, L., Pena, A. J.,
792 Raffanetti, K., Seo, S., Si, M., Thakur, R., Zhang, J., and Zhao, X.: MPICH User's Guide
793 Version 3.4, available at: <https://www.mpich.org/static/downloads/3.4/mpich-3.4-userguide.pdf>,
794 2021.
- 795 Appel, K. W., Napelenok, S. L., Foley, K. M., Pye, H. O. T., Hogrefe, C., Luecken, D. J., Bash, J.
796 O., Roselle, S. J., Pleim, J. E., Foroutan, H., Hutzell, W. T., Pouliot, G. A., Sarwar, G., Fahey, K.
797 M., Gantt, B., Gilliam, R. C., Heath, N. K., Kang, D., Mathur, R., and Schwede, D. B.: Description
798 and evaluation of the Community Multiscale Air Quality (CMAQ) modeling system version 5.1,
799 Geoscientific Model Development, 10, 1703–1732, <https://doi.org/10.5194/gmd-10-1703-2017>,
800 2017.
- 801 Appel, K. W., Bash, J. O., Fahey, K. M., Foley, K. M., Gilliam, R. C., Hogrefe, C., Hutzell, W. T.,
802 Kang, D., Mathur, R., Murphy, B. N., Napelenok, S. L., Nolte, C. G., Pleim, J. E., Pouliot, G. A.,
803 Pye, H. O. T., Ran, L., Roselle, S. J., Sarwar, G., Schwede, D. B., Sidi, F. I., Spero, T. L., and
804 Wong, D. C.: The Community Multiscale Air Quality (CMAQ) model versions 5.3 and 5.3.1:
805 system updates and evaluation, Geoscientific Model Development, 14, 2867–2897,
806 <https://doi.org/10.5194/gmd-14-2867-2021>, 2021.
- 807 Bai, X., Tian, H., Liu, X., Wu, B., Liu, S., Hao, Y., Luo, L., Liu, W., Zhao, S., Lin, S., Hao, J., Guo,
808 Z., and Lv, Y.: Spatial-temporal variation characteristics of air pollution and apportionment of
809 contributions by different sources in Shanxi province of China, Atmospheric Environment, 244,
810 117926, <https://doi.org/10.1016/j.atmosenv.2020.117926>, 2021.
- 811 Cao, K., Wu, Q., Wang, L., Wang, N., Cheng, H., Tang, X., Li, D., and Wang, L.: GPU-HADVPPM
812 V1.0: a high-efficiency parallel GPU design of the piecewise parabolic method (PPM) for
813 horizontal advection in an air quality model (CAMx V6.10), Geosci. Model Dev., 16, 4367–4383,
814 <https://doi.org/10.5194/gmd-16-4367-2023>, 2023.
- 815 Chen, H. S., Wang, Z. F., Li, J., Tang, X., Ge, B. Z., Wu, X. L., Wild, O., and Carmichael, G. R.:
816 GNAQPMS-Hg v1.0, a global nested atmospheric mercury transport model: model description,
817 evaluation and application to trans-boundary transport of Chinese anthropogenic emissions,
818 Geoscientific Model Development, 8, 2857–2876, <https://doi.org/10.5194/gmd-8-2857-2015>,
819 2015.
- 820 George, A. D.: An overview of RISC vs. CISC, in: [1990] Proceedings. The Twenty-Second
821 Southeastern Symposium on System Theory, The Twenty-Second Southeastern Symposium on
822 System Theory, Cookeville, TN, USA, 436–438, <https://doi.org/10.1109/SSST.1990.138185>,
823 1990.

824 Hennessy, J., Jouppi, N., Przybylski, S., Rowen, C., Gross, T., Baskett, F., and Gill, J.: MIPS: A
825 microprocessor architecture, SIGMICRO Newsl., 13, 17–22,
826 <https://doi.org/10.1145/1014194.800930>, 1982.

827 Hu, W., Wang, J., Gao, X., Chen, Y., Liu, Q., and Li, G.: Godson-3: A Scalable Multicore RISC
828 Processor with x86 Emulation, IEEE Micro, 29, 17–29, <https://doi.org/10.1109/MM.2009.30>,
829 2009.

830 Hu, W., Zhang, Y., and Fu, J.: An introduction to CPU and DSP design in China, Sci. China Inf. Sci.,
831 59, 1–8, <https://doi.org/10.1007/s11432-015-5431-6>, 2016.

832 Hu, W., Gao, X., and Zhang, G.: Building the software ecosystem for the Loongson instruction set
833 architecture, Information and Communications Technology and Policy, 43–48, 2022 (in Chinese).

834 Hu, W.-W., Gao, Y.-P., Chen, T.-S., and Xiao, J.-H.: The Godson Processors: Its Research,
835 Development, and Contributions, J. Comput. Sci. Technol., 26, 363–372,
836 <https://doi.org/10.1007/s11390-011-1139-2>, 2011.

837 Intel Inc.: Intel® 64 and IA-32 Architectures Software Developer’s Manual, Volume 1: Ba
838 sic Architecture, available at: [https://www.intel.com/content/www/us/en/developer/articles/te
839 chnical/intel-sdm.html](https://www.intel.com/content/www/us/en/developer/articles/technical/intel-sdm.html), 2023.

840 Li, L., Chen, Z., and Wang, S.: Power Consumption and Analysis of Server Based on Loongson
841 CPU No. 3, Information Technology & Standardization, 46–50, 2014 (in Chinese).

842 Liu, Y., Ye, K., and Xu, C.-Z.: Performance Evaluation of Various RISC Processor Systems: A Case
843 Study on ARM, MIPS and RISC-V, in: Cloud Computing – CLOUD 2021, Cham, 61–74,
844 https://doi.org/10.1007/978-3-030-96326-2_5, 2022.

845 Luo, Q., Kong, C., Cai, Y., and Liu, G.: Performance Evaluation of OpenMP Constructs and Kernel
846 Benchmarks on a Loongson-3A Quad-Core SMP System, in: 2011 12th International Conference
847 on Parallel and Distributed Computing, Applications and Technologies, 2011 12th International
848 Conference on Parallel and Distributed Computing, Applications and Technologies, 191–196,
849 <https://doi.org/10.1109/PDCAT.2011.66>, 2011.

850 Mallach, E. G.: RISC: Evaluation and Selection, Journal of Information Systems Management, 8,
851 8–16, <https://doi.org/10.1080/07399019108964978>, 1991.

852 Michalakes, J., Chen, S., Dudhia, J., Hart, L., Klemp, J., Middlecoff, J., and Skamarock, W.:
853 Development of a next-generation regional weather research and forecast model, in:
854 Developments in Teracomputing, WORLD SCIENTIFIC, 269–276,
855 https://doi.org/10.1142/9789812799685_0024, 2001.

856 MIPS Technology Inc.: MIPS Architecture For Programmers Volume I-A, available at:
857 <https://www.mips.com/products/architectures/mips64>, 2014.

858 Pepe, N., Pirovano, G., Lonati, G., Balzarini, A., Toppetti, A., Riva, G. M., and Bedogni, M.:
859 Development and application of a high resolution hybrid modelling system for the evaluation of
860 urban air quality, Atmospheric Environment, 141, 297–311,
861 <https://doi.org/10.1016/j.atmosenv.2016.06.071>, 2016.

862 Powers, J. G., Klemp, J. B., Skamarock, W. C., Davis, C. A., Dudhia, J., Gill, D. O., Coen, J. L.,
863 Gochis, D. J., Ahmadov, R., Peckham, S. E., Grell, G. A., Michalakes, J., Trahan, S., Benjamin,
864 S. G., Alexander, C. R., Dimego, G. J., Wang, W., Schwartz, C. S., Romine, G. S., Liu, Z., Snyder,
865 C., Chen, F., Barlage, M. J., Yu, W., and Duda, M. G.: The Weather Research and Forecasting
866 Model: Overview, System Efforts, and Future Directions, Bulletin of the American
867 Meteorological Society, 98, 1717–1737, <https://doi.org/10.1175/BAMS-D-15-00308.1>, 2017.

Deleted: Guo, L. and Liu, Y.: Efficient Implementation of FFT on Loongson 3A CPU, Journal of Chinese Computer Systems, 33, 594–597, 2012 (in Chinese).¶

Deleted: Li, L., Chen, Y.-J., Liu, D.-F., Qian, C., and Hu, W.-W.: An FFT Performance Model for Optimizing General-Purpose Processor Architecture, J. Comput. Sci. Technol., 26, 875–889, <https://doi.org/10.1007/s11390-011-0186-z>, 2011.¶

876 RAMBOLL ENVIRON Inc.: CAMx User's Guide Version 6.1, available at: <https://camx->
877 [wp.azurewebsites.net/Files/CAMxUsersGuide_v6.10.pdf](https://camx-azurewebsites.net/Files/CAMxUsersGuide_v6.10.pdf), 2014.

878 Shi, Z.: Technology comparison and research of RISC and CISC, China Science and Technology
879 Information, 131–132, 2008 (in Chinese).

880 Skamarock, C., Klemp, B., Dudhia, J., Gill, O., Liu, Z., Berner, J., Wang, W., Powers, G., Duda, G.,
881 Barker, D., and Huang, X.: A Description of the Advanced Research WRF Model Version 4,
882 <https://doi.org/10.5065/1dfh-6p97>, 2019.

883 Sun Y.: Research on the contribution of soil fugitive dust in Beijing based on satellite identification
884 and numerical simulation technology, Master, Beijing Normal University, <https://etdlib.bnu.edu.cn>,
885 2022a.

886 Sun, Y., Wu, Q., Wang, L., Zhang, B., Yan, P., Wang, L., Cheng, H., Lv, M., Wang, N., and Ma, S.:
887 Weather Reduced the Annual Heavy Pollution Days after 2016 in Beijing, Sola, 18, 135–139,
888 <https://doi.org/10.2151/sola.2022-022>, 2022b.

889 The HDF Group: HDF5 User's Guide Version 1.1, available at:
890 <https://portal.hdfgroup.org/display/HDF5/HDF5+User+Guides>, 2019.

891 UCAR/Unidata: NetCDF User's Guide Version 1.1, available at: <https://docs.unidata.ucar.edu/nug> ,
892 2021.

893 [Wang, H., Lin, J., Wu, Q., Chen, H., Tang, X., Wang, Z., Chen, X., Cheng, H., and Wang, L.: MP](https://doi.org/10.5194/gmd-12-749-2019)
894 [CBM-Z V1.0: design for a new Carbon Bond Mechanism Z \(CBM-Z\) gas-phase chemical](https://doi.org/10.5194/gmd-12-749-2019)
895 [mechanism architecture for next-generation processors. Geoscientific Model Development, 12,](https://doi.org/10.5194/gmd-12-749-2019)
896 [749–764. https://doi.org/10.5194/gmd-12-749-2019. 2019.](https://doi.org/10.5194/gmd-12-749-2019)

897 Wang, K., Gao, C., Wu, K., Liu, K., Wang, H., Dan, M., Ji, X., and Tong, Q.: ISAT v2.0: an
898 integrated tool for nested-domain configurations and model-ready emission inventories for WRF-
899 AQM, Geoscientific Model Development, 16, 1961–1973, [https://doi.org/10.5194/gmd-16-1961-](https://doi.org/10.5194/gmd-16-1961-2023)
900 [2023](https://doi.org/10.5194/gmd-16-1961-2023), 2023.

901 Wang, P., Jiang, J., Lin, P., Ding, M., Wei, J., Zhang, F., Zhao, L., Li, Y., Yu, Z., Zheng, W., Yu, Y.,
902 Chi, X., and Liu, H.: The GPU version of LASG/IAP Climate System Ocean Model version 3
903 (LICOM3) under the heterogeneous-compute interface for portability (HIP) framework and its
904 large-scale application, Geosci. Model Dev., 14, 2781–2799, [https://doi.org/10.5194/gmd-14-](https://doi.org/10.5194/gmd-14-2781-2021)
905 [2781-2021](https://doi.org/10.5194/gmd-14-2781-2021), 2021.

906 Wang, S., Li, L., and Chen, Z.: The Test and Analysis on Memory Access Performance Based on
907 Loongson CPU, Information Technology & Standardization, 32–36, 2014 (in Chinese).

908 Wang, Z., Xie, F., Wang, X., An, J., and Zhu, J.: Development and Application of Nested Air Quality
909 Prediction Modeling System, Chinese Journal of Atmospheric Sciences, 778–790,
910 <http://dx.doi.org/10.3878/j.issn.1006-9895.2006.05.07>, 2006.

911 Wu, Q. and Cheng, H.: Transplantation and application of mesoscale mode on Loongson CPU
912 platform, Journal of Beijing Normal University (Natural Science), 55, 11–18,
913 <https://doi.org/10.16360/j.cnki.jbnuns.2019.01.002>, 2019.

914 Wu, Q., Xu, W., Shi, A., Li, Y., Zhao, X., Wang, Z., Li, J., and Wang, L.: Air quality forecast of
915 PM10 in Beijing with Community Multi-scale Air Quality Modeling (CMAQ) system: emission
916 and improvement, Geoscientific Model Development, 7, 2243–2259,
917 <https://doi.org/10.5194/gmd-7-2243-2014>, 2014.

918 Wu, Y., Xu, G., Zhao, Y., and Tan, Y.: Parallel Processing on WRF Meteorological Data Using
919 MPICH, in: 2012 Sixth International Conference on Internet Computing for Science and

920 Engineering, 2012 Sixth International Conference on Internet Computing for Science and
921 Engineering, titleTranslation:, 262–265, <https://doi.org/10.1109/ICICSE.2012.12>, 2012.

922 Xiao, H., Wu, Q., Yang, X., Wang, L., and Cheng, H.: Numerical study of the effects of initial
923 conditions and emissions on PM2.5 concentration simulations with CAMx v6.1: a Xi'an case
924 study, *Geoscientific Model Development*, 14, 223–238, [https://doi.org/10.5194/gmd-14-223-](https://doi.org/10.5194/gmd-14-223-2021)
925 [2021](https://doi.org/10.5194/gmd-14-223-2021), 2021.

926 Yang, X., Xiao, H., Wu, Q., Wang, L., Guo, Q., Cheng, H., Wang, R., and Tang, Z.: Numerical study
927 of air pollution over a typical basin topography: Source appointment of fine particulate matter
928 during one severe haze in the megacity Xi'an, *Science of The Total Environment*, 708, 135213,
929 <https://doi.org/10.1016/j.scitotenv.2019.135213>, 2020.

930 Zhang, Y., Bocquet, M., Mallet, V., Seigneur, C., and Baklanov, A.: Real-time air quality forecasting,
931 part I: History, techniques, and current status, *Atmospheric Environment*, 60, 632–655,
932 <https://doi.org/10.1016/j.atmosenv.2012.06.031>, 2012.

933 Zhang, Z., Wang, X., Cheng, S., Guan, P., Zhang, H., Shan, C., and Fu, Y.: Investigation on the
934 difference of PM2.5 transport flux between the North China Plain and the Sichuan Basin,
935 *Atmospheric Environment*, 271, 118922, <https://doi.org/10.1016/j.atmosenv.2021.118922>, 2022.

936 Zhen, J., Guan, P., Yang, R., and Zhai, M.: Transport matrix of PM2.5 in Beijing-Tianjin-Hebei and
937 Yangtze River Delta regions: Assessing the contributions from emission reduction and
938 meteorological conditions, *Atmospheric Environment*, 304, 119775,
939 <https://doi.org/10.1016/j.atmosenv.2023.119775>, 2023.

940 Zhi, Y. and Xu, J.: Android transplantation and analysis based on Loongson, in: 2012 International
941 Conference on Information Management, Innovation Management and Industrial Engineering,
942 2012 International Conference on Information Management, Innovation Management and
943 Industrial Engineering, 59–61, <https://doi.org/10.1109/ICIII.2012.6339777>, 2012.

Deleted: Zhao, M., Zhang, Y., Liu, Y., Li, Y., and Yan, S.:
Comparison and Analysis of Three Types of FFT Adaptive
Libraries on Loongson 3A, *Computer Science*, 39, 281–285,
2012 (in Chinese).¶

Page 10: [1] Deleted Zehua Bai 2/28/24 3:22:00 AM

Page 11: [2] Deleted Zehua Bai 2/28/24 3:33:00 AM

Page 12: [3] Deleted Zehua Bai 2/28/24 3:50:00 AM